Recovering High Dynamic Range Radiance Maps from Photographs

Paul E. Debevec   Jitendra Malik

University of California at Berkeley[1]

ABSTRACT

We present a method of recovering high dynamic range radiance maps from photographs taken with conventional imaging equipment. In our method, multiple photographs of the scene are taken with different amounts of exposure. Our algorithm uses these differently exposed photographs to recover the response function of the imaging process, up to factor of scale, using the assumption of reciprocity. With the known response function, the algorithm can fuse the multiple photographs into a single, high dynamic range radiance map whose pixel values are proportional to the true radiance values in the scene. We demonstrate our method on images acquired with both photochemical and digital imaging processes. We discuss how this work is applicable in many areas of computer graphics involving digitized photographs, including image-based modeling, image compositing, and image processing. Lastly, we demonstrate a few applications of having high dynamic range radiance maps, such as synthesizing realistic motion blur and simulating the response of the human visual system.

CR Descriptors: I.2.10 [**Artificial Intelligence**]: Vision and Scene Understanding - *Intensity, color, photometry and thresholding*; I.3.7 [**Computer Graphics**]: Three-Dimensional Graphics and Realism - *Color, shading, shadowing, and texture*; I.4.1 [**Image Processing**]: Digitization - *Scanning*; I.4.8 [**Image Processing**]: Scene Analysis - *Photometry, Sensor Fusion*.

1 Introduction

Digitized photographs are becoming increasingly important in computer graphics. More than ever, scanned images are used as texture maps for geometric models, and recent work in image-based modeling and rendering uses images as the fundamental modeling primitive. Furthermore, many of today's graphics applications require computer-generated images to mesh seamlessly with real photographic imagery. Properly using photographically acquired imagery in these applications can greatly benefit from an accurate model of the photographic process.

When we photograph a scene, either with film or an electronic imaging array, and digitize the photograph to obtain a two-dimensional array of "brightness" values, these values are rarely true measurements of relative radiance in the scene. For example, if one pixel has twice the value of another, it is unlikely that it observed twice the radiance. Instead, there is usually an unknown, nonlinear mapping that determines how radiance in the scene becomes pixel values in the image.

This nonlinear mapping is hard to know beforehand because it is actually the composition of several nonlinear mappings that occur in the photographic process. In a conventional camera (see Fig. 1), the film is first exposed to light to form a latent image. The film is then developed to change this latent image into variations in transparency, or *density*, on the film. The film can then be digitized using a film scanner, which projects light through the film onto an electronic light-sensitive array, converting the image to electrical voltages. These voltages are digitized, and then manipulated before finally being written to the storage medium. If prints of the film are scanned rather than the film itself, then the printing process can also introduce nonlinear mappings.

In the first stage of the process, the film response to variations in exposure X (which is $E\Delta t$, the product of the irradiance E the film receives and the exposure time Δt) is a non-linear function, called the "characteristic curve" of the film. Noteworthy in the typical characteristic curve is the presence of a small response with no exposure and saturation at high exposures. The development, scanning and digitization processes usually introduce their own nonlinearities which compose to give the aggregate nonlinear relationship between the image pixel exposures X and their values Z.

Digital cameras, which use charge coupled device (CCD) arrays to image the scene, are prone to the same difficulties. Although the charge collected by a CCD element is proportional to its irradiance, most digital cameras apply a nonlinear mapping to the CCD outputs before they are written to the storage medium. This nonlinear mapping is used in various ways to mimic the response characteristics of film, anticipate nonlinear responses in the display device, and often to convert 12-bit output from the CCD's analog-to-digital converters to 8-bit values commonly used to store images. As with film, the most significant nonlinearity in the response curve is at its saturation point, where any pixel with a radiance above a certain level is mapped to the same maximum image value.

Why is this any problem at all? The most obvious difficulty, as any amateur or professional photographer knows, is that of limited dynamic range—one has to choose the range of radiance values that are of interest and determine the exposure time suitably. Sunlit scenes, and scenes with shiny materials and artificial light sources, often have extreme differences in radiance values that are impossible to capture without either under-exposing or saturating the film. To cover the full dynamic range in such a scene, one can take a series of photographs with different exposures. This then poses a problem: how can we combine these separate images into a composite radiance map? Here the fact that the mapping from scene radiance to pixel values is unknown and nonlinear begins to haunt us. The purpose of this paper is to present a simple technique for recovering this response function, up to a scale factor, using nothing more than a set of photographs taken with varying, known exposure durations. With this mapping, we then use the pixel values from all available photographs to construct an accurate map of the radiance in the scene, up to a factor of scale. This radiance map will cover
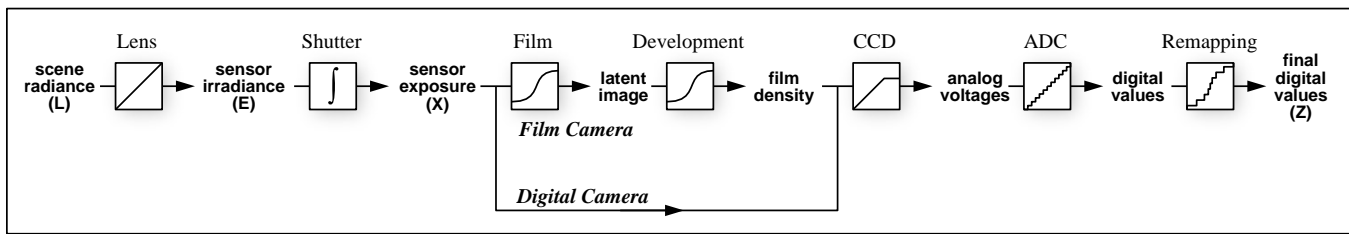
Figure 1: **Image Acquisition Pipeline** *shows how scene radiance becomes pixel values for both film and digital cameras. Unknown nonlinear mappings can occur during exposure, development, scanning, digitization, and remapping. The algorithm in this paper determines the aggregate mapping from scene radiance L to pixel values Z from a set of differently exposed images.*

the entire dynamic range captured by the original photographs.

1.1 Applications

Our technique of deriving imaging response functions and recovering high dynamic range radiance maps has many possible applications in computer graphics:

Image-based modeling and rendering

Image-based modeling and rendering systems to date (e.g. [11, 15, 2, 3, 12, 6, 17]) make the assumption that all the images are taken with the same exposure settings and film response functions. However, almost any large-scale environment will have some areas that are much brighter than others, making it impossible to adequately photograph the scene using a single exposure setting. In indoor scenes with windows, this situation often arises within the field of view of a single photograph, since the areas visible through the windows can be far brighter than the areas inside the building.

By determining the response functions of the imaging device, the method presented here allows one to correctly fuse pixel data from photographs taken at different exposure settings. As a result, one can properly photograph outdoor areas with short exposures, and indoor areas with longer exposures, without creating inconsistencies in the data set. Furthermore, knowing the response functions can be helpful in merging photographs taken with different imaging systems, such as video cameras, digital cameras, and film cameras with various film stocks and digitization processes.

The area of image-based modeling and rendering is working toward recovering more advanced reflection models (up to complete BRDF's) of the surfaces in the scene (e.g. [21]). These methods, which involve observing surface radiance in various directions under various lighting conditions, require absolute radiance values rather than the nonlinearly mapped pixel values found in conventional images. Just as important, the recovery of high dynamic range images will allow these methods to obtain accurate radiance values from surface specularities and from incident light sources. Such higher radiance values usually become clamped in conventional images.

Image processing

Most image processing operations, such as blurring, edge detection, color correction, and image correspondence, expect pixel values to be proportional to the scene radiance. Because of nonlinear image response, especially at the point of saturation, these operations can produce incorrect results for conventional images.

In computer graphics, one common image processing operation is the application of synthetic motion blur to images. In our results (Section 3), we will show that using true radiance maps produces significantly more realistic motion blur effects for high dynamic range scenes.

Image compositing

Many applications in computer graphics involve compositing image data from images obtained by different processes. For example, a background matte might be shot with a still camera, live action might be shot with a different film stock or scanning process, and CG elements would be produced by rendering algorithms. When there are significant differences in the response curves of these imaging processes, the composite image can be visually unconvincing. The technique presented in this paper provides a convenient and robust method of determining the overall response curve of any imaging process, allowing images from different processes to be used consistently as radiance maps. Furthermore, the recovered response curves can be inverted to render the composite radiance map as if it had been photographed with any of the original imaging processes, or a different imaging process entirely.

A research tool

One goal of computer graphics is to simulate the image formation process in a way that produces results that are consistent with what happens in the real world. Recovering radiance maps of real-world scenes should allow more quantitative evaluations of rendering algorithms to be made in addition to the qualitative scrutiny they traditionally receive. In particular, the method should be useful for developing reflectance and illumination models, and comparing global illumination solutions against ground truth data.

Rendering high dynamic range scenes on conventional display devices is the subject of considerable previous work, including [20, 16, 5, 23]. The work presented in this paper will allow such methods to be tested on real radiance maps in addition to synthetically computed radiance solutions.

1.2 Background

The photochemical processes involved in silver halide photography have been the subject of continued innovation and research ever since the invention of the daguerretype in 1839. [18] and [8] provide a comprehensive treatment of the theory and mechanisms involved. For the newer technology of solid-state imaging with charge coupled devices, [19] is an excellent reference. The technical and artistic problem of representing the dynamic range of a natural scene on the limited range of film has concerned photographers from the early days – [1] presents one of the best known systems to choose shutter speeds, lens apertures, and developing conditions to best coerce the dynamic range of a scene to fit into what is possible on a print. In scientific applications of photography, such as in astronomy, the nonlinear film response has been addressed by suitable calibration procedures. It is our objective instead to develop a simple self-calibrating procedure not requiring calibration charts or photometric measuring devices.

In previous work, [13] used multiple flux integration times of a CCD array to acquire extended dynamic range images. Since direct CCD outputs were available, the work did not need to deal with the

problem of nonlinear pixel value response. [14] addressed the problem of nonlinear response but provide a rather limited method of recovering the response curve. Specifically, a parametric form of the response curve is arbitrarily assumed, there is no satisfactory treatment of image noise, and the recovery process makes only partial use of the available data.

2   The Algorithm

This section presents our algorithm for recovering the film response function, and then presents our method of reconstructing the high dynamic range radiance image from the multiple photographs. We describe the algorithm assuming a grayscale imaging device. We discuss how to deal with color in Section 2.6.

2.1   Film Response Recovery

Our algorithm is based on exploiting a physical property of imaging systems, both photochemical and electronic, known as *reciprocity*.

Let us consider photographic film first. The response of a film to variations in exposure is summarized by the characteristic curve (or Hurter-Driffield curve). This is a graph of the optical density D of the processed film against the logarithm of the exposure X to which it has been subjected. The exposure X is defined as the product of the irradiance E at the film and exposure time, Δt, so that its units are Jm^{-2}. Key to the very concept of the characteristic curve is the assumption that only the product $E\Delta t$ is important, that halving E and doubling Δt will not change the resulting optical density D. Under extreme conditions (very large or very low Δt), the reciprocity assumption can break down, a situation described as reciprocity failure. In typical print films, reciprocity holds to within $\frac{1}{3}$ stop[1] for exposure times of 10 seconds to 1/10,000 of a second.[2] In the case of charge coupled arrays, reciprocity holds under the assumption that each site measures the total number of photons it absorbs during the integration time.

After the development, scanning and digitization processes, we obtain a digital number Z, which is a nonlinear function of the original exposure X at the pixel. Let us call this function f, which is the composition of the characteristic curve of the film as well as all the nonlinearities introduced by the later processing steps. Our first goal will be to recover this function f. Once we have that, we can compute the exposure X at each pixel, as $X = f^{-1}(Z)$. We make the reasonable assumption that the function f is monotonically increasing, so its inverse f^{-1} is well defined. Knowing the exposure X and the exposure time Δt, the irradiance E is recovered as $E = X/\Delta t$, which we will take to be proportional to the radiance L in the scene.[3]

Before proceeding further, we should discuss the consequences of the spectral response of the sensor. The exposure X should be thought of as a function of wavelength $X(\lambda)$, and the abscissa on the characteristic curve should be the integral $\int X(\lambda)R(\lambda)d\lambda$ where $R(\lambda)$ is the spectral response of the sensing element at the pixel location. Strictly speaking, our use of irradiance, a radiometric quantity, is not justified. However, the spectral response of the sensor site may not be the photopic luminosity function V_λ, so the photometric term *illuminance* is not justified either. In what follows, we will use the term irradiance, while urging the reader to remember that the

quantities we will be dealing with are weighted by the spectral response at the sensor site. For color photography, the color channels may be treated separately.

The input to our algorithm is a number of digitized photographs taken from the same vantage point with different known exposure durations Δt_j.[4] We will assume that the scene is static and that this process is completed quickly enough that lighting changes can be safely ignored. It can then be assumed that the film irradiance values E_i for each pixel i are constant. We will denote pixel values by Z_{ij} where i is a spatial index over pixels and j indexes over exposure times Δt_j. We may now write down the film reciprocity equation as:

$$Z_{ij} = f(E_i \Delta t_j) \tag{1}$$

Since we assume f is monotonic, it is invertible, and we can rewrite (1) as:

$$f^{-1}(Z_{ij}) = E_i \Delta t_j$$

Taking the natural logarithm of both sides, we have:

$$\ln f^{-1}(Z_{ij}) = \ln E_i + \ln \Delta t_j$$

To simplify notation, let us define function $g = \ln f^{-1}$. We then have the set of equations:

$$g(Z_{ij}) = \ln E_i + \ln \Delta t_j \tag{2}$$

where i ranges over pixels and j ranges over exposure durations. In this set of equations, the Z_{ij} are known, as are the Δt_j. The unknowns are the irradiances E_i, as well as the function g, although we assume that g is smooth and monotonic.

We wish to recover the function g and the irradiances E_i that best satisfy the set of equations arising from Equation 2 in a least-squared error sense. We note that recovering g only requires recovering the *finite* number of values that $g(z)$ can take since the domain of Z, pixel brightness values, is finite. Letting Z_{min} and Z_{max} be the least and greatest pixel values (integers), N be the number of pixel locations and P be the number of photographs, we formulate the problem as one of finding the $(Z_{max} - Z_{min} + 1)$ values of $g(Z)$ and the N values of $\ln E_i$ that minimize the following quadratic objective function:

$$\mathcal{O} = \sum_{i=1}^{N} \sum_{j=1}^{P} [g(Z_{ij}) - \ln E_i - \ln \Delta t_j]^2 + \lambda \sum_{z=Z_{min}+1}^{Z_{max}-1} g''(z)^2 \tag{3}$$

The first term ensures that the solution satisfies the set of equations arising from Equation 2 in a least squares sense. The second term is a smoothness term on the sum of squared values of the second derivative of g to ensure that the function g is smooth; in this discrete setting we use $g''(z) = g(z-1) - 2g(z) + g(z+1)$. This smoothness term is essential to the formulation in that it provides coupling between the values $g(z)$ in the minimization. The scalar λ weights the smoothness term relative to the data fitting term, and should be chosen appropriately for the amount of noise expected in the Z_{ij} measurements.

Because it is quadratic in the E_i's and $g(z)$'s, minimizing $\mathcal{O}$ is a straightforward linear least squares problem. The overdetermined

---

[1] 1 stop is a photographic term for a factor of two; $\frac{1}{3}$ stop is thus $2^{\frac{1}{3}}$

[2] An even larger dynamic range can be covered by using neutral density filters to lessen to amount of light reaching the film for a given exposure time. A discussion of the modes of reciprocity failure may be found in [18], ch. 4.

[3] L is proportional E for any particular pixel, but it is possible for the proportionality factor to be different at different places on the sensor. One formula for this variance, given in [7], is $E = L \frac{\pi}{4} \left(\frac{d}{f} \right)^2 cos^4 \alpha$, where α measures the pixel's angle from the lens' optical axis. However, most modern camera lenses are designed to compensate for this effect, and provide a nearly constant mapping between radiance and irradiance at f/8 and smaller apertures. See also [10].

[4] Most modern SLR cameras have electronically controlled shutters which give extremely accurate and reproducible exposure times. We tested our Canon EOS Elan camera by using a Macintosh to make digital audio recordings of the shutter. By analyzing these recordings we were able to verify the accuracy of the exposure times to within a thousandth of a second. Conveniently, we determined that the actual exposure times varied by powers of two between stops ($\frac{1}{64}, \frac{1}{32}, \frac{1}{16}, \frac{1}{8}, \frac{1}{4}, \frac{1}{2}$, 1, 2, 4, 8, 16, 32), rather than the rounded numbers displayed on the camera readout ($\frac{1}{60}, \frac{1}{30}, \frac{1}{15}, \frac{1}{8}$, $\frac{1}{4}, \frac{1}{2}$, 1, 2, 4, 8, 15, 30). Because of problems associated with vignetting, varying the aperture is not recommended.

system of linear equations is robustly solved using the singular value decomposition (SVD) method. An intuitive explanation of the procedure may be found in Fig. 2.

We need to make three additional points to complete our description of the algorithm:

First, the solution for the $g(z)$ and E_i values can only be up to a single scale factor α. If each log irradiance value $\ln E_i$ were replaced by $\ln E_i + \alpha$, and the function g replaced by $g + \alpha$, the system of equations 2 and also the objective function $\mathcal{O}$ would remain unchanged. To establish a scale factor, we introduce the additional constraint $g(Z_{mid}) = 0$, where $Z_{mid} = \frac{1}{2}(Z_{min} + Z_{max})$, simply by adding this as an equation in the linear system. The meaning of this constraint is that a pixel with value midway between Z_{min} and Z_{max} will be assumed to have unit exposure.

Second, the solution can be made to have a much better fit by anticipating the basic shape of the response function. Since $g(z)$ will typically have a steep slope near Z_{min} and Z_{max}, we should expect that $g(z)$ will be less smooth and will fit the data more poorly near these extremes. To recognize this, we can introduce a weighting function $w(z)$ to emphasize the smoothness and fitting terms toward the middle of the curve. A sensible choice of w is a simple hat function:

$$w(z) = \begin{cases} z - Z_{min} & \text{for } z \leq \frac{1}{2}(Z_{min} + Z_{max}) \\ Z_{max} - z & \text{for } z > \frac{1}{2}(Z_{min} + Z_{max}) \end{cases} \quad (4)$$

Equation 3 now becomes:

$$\mathcal{O} = \sum_{i=1}^{N} \sum_{j=1}^{P} \left\{ w(Z_{ij}) \left[g(Z_{ij}) - \ln E_i - \ln \Delta t_j \right] \right\}^2 +$$

$$\lambda \sum_{z=Z_{min}+1}^{Z_{max}-1} \left[w(z) g''(z) \right]^2$$

Finally, we need not use every available pixel site in this solution procedure. Given measurements of N pixels in P photographs, we have to solve for N values of $\ln E_i$ and $(Z_{max} - Z_{min})$ samples of g. To ensure a sufficiently overdetermined system, we want $N(P-1) > (Z_{max} - Z_{min})$. For the pixel value range $(Z_{max} - Z_{min}) = 255$, $P = 11$ photographs, a choice of N on the order of 50 pixels is more than adequate. Since the size of the system of linear equations arising from Equation 3 is on the order of $N \times P + Z_{max} - Z_{min}$, computational complexity considerations make it impractical to use every pixel location in this algorithm. Clearly, the pixel locations should be chosen so that they have a reasonably even distribution of pixel values from Z_{min} to Z_{max}, and so that they are spatially well distributed in the image. Furthermore, the pixels are best sampled from regions of the image with low intensity variance so that radiance can be assumed to be constant across the area of the pixel, and the effect of optical blur of the imaging system is minimized. So far we have performed this task by hand, though it could easily be automated.

Note that we have not explicitly enforced the constraint that g must be a monotonic function. If desired, this can be done by transforming the problem to a non-negative least squares problem. We have not found it necessary because, in our experience, the smoothness penalty term is enough to make the estimated g monotonic in addition to being smooth.

To show its simplicity, the MATLAB routine we used to minimize Equation 5 is included in the Appendix. Running times are on the order of a few seconds.

2.2 Constructing the High Dynamic Range Radiance Map

Once the response curve g is recovered, it can be used to quickly convert pixel values to relative radiance values, assuming the exposure Δt_j is known. Note that the curve can be used to determine radiance values in any image(s) acquired by the imaging process associated with g, not just the images used to recover the response function.

From Equation 2, we obtain:

$$\ln E_i = g(Z_{ij}) - \ln \Delta t_j \quad (5)$$

For robustness, and to recover high dynamic range radiance values, we should use all the available exposures for a particular pixel to compute its radiance. For this, we reuse the weighting function in Equation 4 to give higher weight to exposures in which the pixel's value is closer to the middle of the response function:

$$\ln E_i = \frac{\sum_{j=1}^{P} w(Z_{ij})(g(Z_{ij}) - \ln \Delta t_j)}{\sum_{j=1}^{P} w(Z_{ij})} \quad (6)$$

Combining the multiple exposures has the effect of reducing noise in the recovered radiance values. It also reduces the effects of imaging artifacts such as film grain. Since the weighting function ignores saturated pixel values, "blooming" artifacts[5] have little impact on the reconstructed radiance values.

2.2.1 Storage

In our implementation the recovered radiance map is computed as an array of single-precision floating point values. For efficiency, the map can be converted to the image format used in the RADIANCE [22] simulation and rendering system, which uses just eight bits for each of the mantissa and exponent. This format is particularly compact for color radiance maps, since it stores just one exponent value for all three color values at each pixel. Thus, in this format, a high dynamic range radiance map requires just one third more storage than a conventional RGB image.

2.3 How many images are necessary?

To decide on the number of images needed for the technique, it is convenient to consider the two aspects of the process:

1. *Recovering the film response curve:* This requires a minimum of two photographs. Whether two photographs are enough can be understood in terms of the heuristic explanation of the process of film response curve recovery shown in Fig. 2. If the scene has sufficiently many different radiance values, the entire curve can, in principle, be assembled by sliding together the sampled curve segments, each with only two samples. Note that the photos must be similar enough in their exposure amounts that some pixels fall into the working range[6] of the film in both images; otherwise, there is no information to relate the exposures to each other. Obviously, using more than two images with differing exposure times improves performance with respect to noise sensitivity.

2. *Recovering a radiance map given the film response curve:* The number of photographs needed here is a function of the dynamic range of radiance values in the scene. Suppose the range of maximum to minimum radiance values that we are

---

[5]Blooming occurs when charge or light at highly saturated sites on the imaging surface spills over and affects values at neighboring sites.

[6]The *working range* of the film corresponds to the middle section of the response curve. The ends of the curve, in which large changes in exposure cause only small changes in density (or pixel value), are called the *toe* and the *shoulder*.
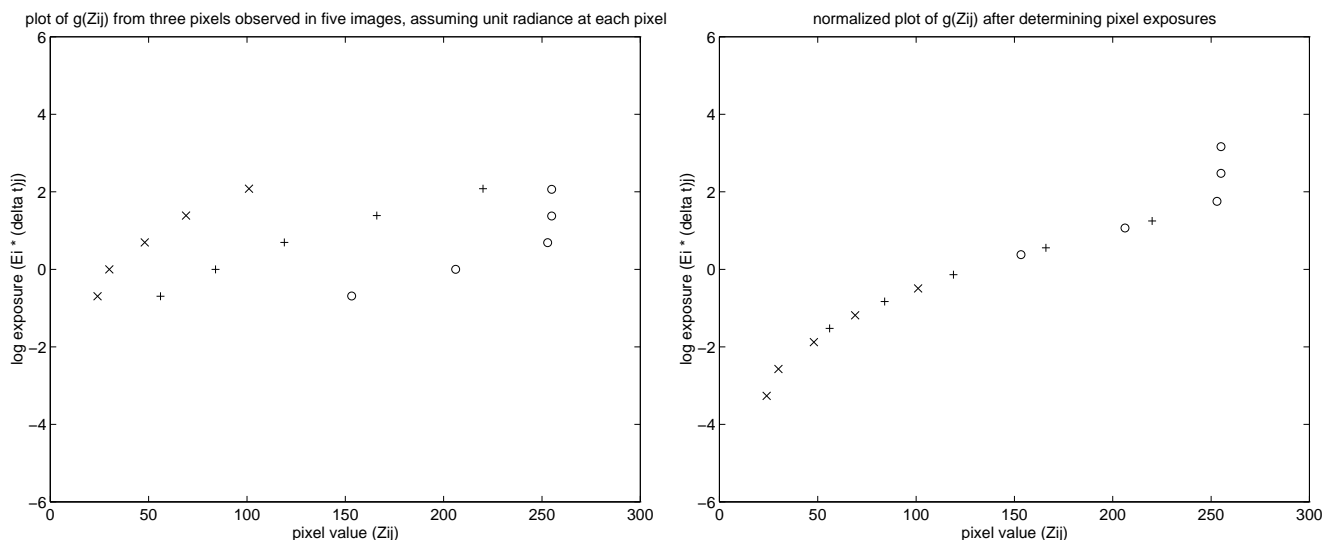
plot of g(Zij) from three pixels observed in five images, assuming unit radiance at each pixel

normalized plot of g(Zij) after determining pixel exposures

Figure 2: *In the figure on the left, the $\times$ symbols represent samples of the g curve derived from the digital values at one pixel for 5 different known exposures using Equation 2. The unknown log irradiance $\ln E_i$ has been arbitrarily assumed to be 0. Note that the shape of the g curve is correct, though its position on the vertical scale is arbitrary corresponding to the unknown $\ln E_i$. The $+$ and $\circ$ symbols show samples of g curve segments derived by consideration of two other pixels; again the vertical position of each segment is arbitrary. Essentially, what we want to achieve in the optimization process is to slide the 3 sampled curve segments up and down (by adjusting their $\ln E_i$'s) until they "line up" into a single smooth, monotonic curve, as shown in the right figure. The vertical position of the composite curve will remain arbitrary.*

interested in recovering accurately is R, and the film is capable of representing in its working range a dynamic range of F. Then the minimum number of photographs needed is $\lceil \frac{R}{F} \rceil$ to ensure that every part of the scene is imaged in at least one photograph at an exposure duration that puts it in the working range of the film response curve. As in recovering the response curve, using more photographs than strictly necessary will result in better noise sensitivity.

If one wanted to use as few photographs as possible, one might first recover the response curve of the imaging process by photographing a scene containing a diverse range of radiance values at three or four different exposures, differing by perhaps one or two stops. This response curve could be used to determine the working range of the imaging process, which for the processes we have seen would be as many as five or six stops. For the remainder of the shoot, the photographer could decide for any particular scene the number of shots necessary to cover its entire dynamic range. For diffuse indoor scenes, only one exposure might be necessary; for scenes with high dynamic range, several would be necessary. By recording the exposure amount for each shot, the images could then be converted to radiance maps using the pre-computed response curve.

2.4 Recovering extended dynamic range from single exposures

Most commericially available film scanners can detect reasonably close to the full range of useful densities present in film. However, many of these scanners (as well as the Kodak PhotoCD process) produce 8-bit-per-channel images designed to be viewed on a screen or printed on paper. Print film, however, records a significantly greater dynamic range than can be displayed with either of these media. As a result, such scanners deliver only a portion of the detected dynamic range of print film in a single scan, discarding information in either high or low density regions. The portion of the detected dynamic range that is delivered can usually be influenced by "brightness" or "density adjustment" controls.

The method presented in this paper enables two methods for recovering the full dynamic range of print film which we will briefly

outline[7]. In the first method, the print negative is scanned with the scanner set to scan slide film. Most scanners will then record the entire detectable dynamic range of the film in the resulting image. As before, a series of differently exposed images of the same scene can be used to recover the response function of the imaging system with each of these scanner settings. This response function can then be used to convert individual exposures to radiance maps. Unfortunately, since the resulting image is still 8-bits-per-channel, this results in increased quantization.

In the second method, the film can be scanned twice with the scanner set to different density adjustment settings. A series of differently exposed images of the same scene can then be used to recover the response function of the imaging system at each of these density adjustment settings. These two response functions can then be used to combine two scans of any single negative using a similar technique as in Section 2.2.

2.5 Obtaining Absolute Radiance

For many applications, such as image processing and image compositing, the relative radiance values computed by our method are all that are necessary. If needed, an approximation to the scaling term necessary to convert to absolute radiance can be derived using the ASA of the film[8] and the shutter speeds and exposure amounts in the photographs. With these numbers, formulas that give an approximate prediction of film response can be found in [9]. Such an approximation can be adequate for simulating visual artifacts such as glare, and predicting areas of scotopic retinal response. If desired, one could recover the scaling factor precisely by photographing a calibration luminaire of known radiance, and scaling the radiance values to agree with the known radiance of the luminaire.

2.6 Color

Color images, consisting of red, green, and blue channels, can be processed by reconstructing the imaging system response curve for

---

[7]This work was done in collaboration with Gregory Ward Larson
[8]Conveniently, most digital cameras also specify their sensitivity in terms of ASA.

each channel independently. Unfortunately, there will be three unknown scaling factors relating relative radiance to absolute radiance, one for each channel. As a result, different choices of these scaling factors will change the color balance of the radiance map.

By default, the algorithm chooses the scaling factor such that a pixel with value Z_{mid} will have unit exposure. Thus, any pixel with the RGB value $(Z_{mid}, Z_{mid}, Z_{mid})$ will have equal radiance values for R, G, and B, meaning that the pixel is achromatic. If the three channels of the imaging system actually do respond equally to achromatic light in the neighborhood of Z_{mid}, then our procedure correctly reconstructs the relative radiances.

However, films are usually calibrated to respond achromatically to a particular color of light C, such as sunlight or fluorescent light. In this case, the radiance values of the three channels should be scaled so that the pixel value $(Z_{mid}, Z_{mid}, Z_{mid})$ maps to a radiance with the same color ratios as C. To properly model the color response of the entire imaging process rather than just the film response, the scaling terms can be adjusted by photographing a calibration luminaire of known color.

2.7 Taking virtual photographs

The recovered response functions can also be used to map radiance values back to pixel values for a given exposure Δt using Equation 1. This process can be thought of as taking a virtual photograph of the radiance map, in that the resulting image will exhibit the response qualities of the modeled imaging system. Note that the response functions used need not be the same response functions used to construct the original radiance map, which allows photographs acquired with one imaging process to be rendered as if they were acquired with another.[9]

3 Results

Figures 3-5 show the results of using our algorithm to determine the response curve of a DCS460 digital camera. Eleven grayscale photographs filtered down to 765×509 resolution (Fig. 3) were taken at f/8 with exposure times ranging from $\frac{1}{30}$ of a second to 30 seconds, with each image receiving twice the exposure of the previous one. The film curve recovered by our algorithm from 45 pixel locations observed across the image sequence is shown in Fig. 4. Note that although CCD image arrays naturally produce linear output, from the curve it is evident that the camera nonlinearly remaps the data, presumably to mimic the response curves found in film. The underlying registered $(E_i \Delta t_j, Z_{ij})$ data are shown as light circles underneath the curve; some outliers are due to sensor artifacts (light horizontal bands across some of the darker images.)

Fig. 5 shows the reconstructed high dynamic range radiance map. To display this map, we have taken the logarithm of the radiance values and mapped the range of these values into the range of the display. In this representation, the pixels at the light regions do not saturate, and detail in the shadow regions can be made out, indicating that all of the information from the original image sequence is present in the radiance map. The large range of values present in the radiance map (over four orders of magnitude of useful dynamic range) is shown by the values at the marked pixel locations.

Figure 6 shows sixteen photographs taken inside a church with a Canon 35mm SLR camera on Fuji 100 ASA color print film. A fisheye 15mm lens set at f/8 was used, with exposure times ranging from 30 seconds to $\frac{1}{1000}$ of a second in 1-stop increments. The film was developed professionally and scanned in using a Kodak PhotoCD film scanner. The scanner was set so that it would not individually

---

[9] Note that here we are assuming that the spectral response functions for each channel of the two imaging processes is the same. Also, this technique does not model many significant qualities of an imaging system such as film grain, chromatic aberration, blooming, and the modulation transfer function.

Figure 3: **(a)** *Eleven grayscale photographs of an indoor scene acquired with a Kodak DCS460 digital camera, with shutter speeds progressing in 1-stop increments from $\frac{1}{30}$ of a second to 30 seconds.*
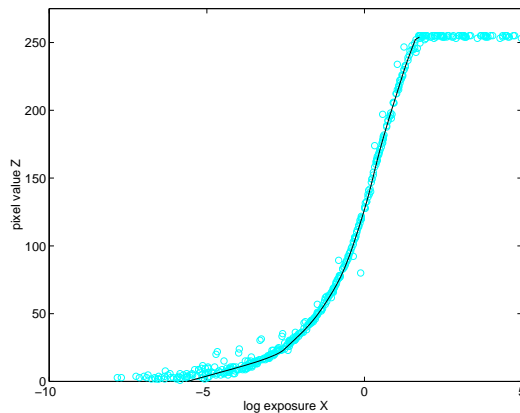

Figure 4: *The response function of the DCS460 recovered by our algorithm, with the underlying $(E_i \Delta t_j, Z_{ij})$ data shown as light circles. The logarithm is base e.*

Figure 5: *The reconstructed high dynamic range radiance map, mapped into a grayscale image by taking the logarithm of the radiance values. The relative radiance values of the marked pixel locations, clockwise from lower left: 1.0, 46.2, 1907.1, 15116.0, and 18.0.*

Figure 6: *Sixteen photographs of a church taken at 1-stop increments from 30 sec to $\frac{1}{1000}$ sec. The sun is directly behind the rightmost stained glass window, making it especially bright. The blue borders seen in some of the image margins are induced by the image registration process.*
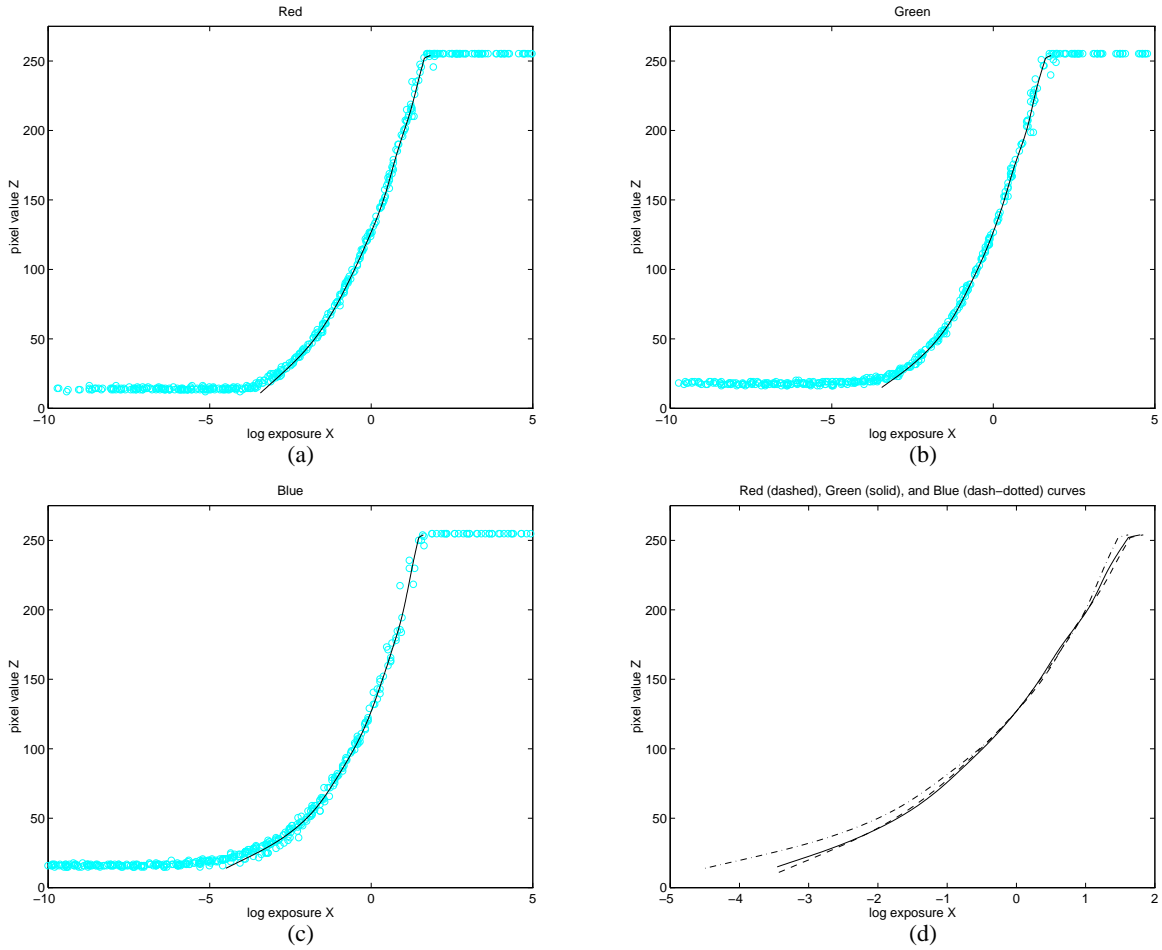

Figure 7: *Recovered response curves for the imaging system used in the church photographs in Fig. 8.* **(a-c)** *Response functions for the red, green, and blue channels, plotted with the underlying $(E_i \Delta t_j, Z_{ij})$ data shown as light circles.* **(d)** *The response functions for red, green, and blue plotted on the same axes. Note that while the red and green curves are very consistent, the blue curve rises significantly above the others for low exposure values. This indicates that dark regions in the images exhibit a slight blue cast. Since this artifact is recovered by the response curves, it does not affect the relative radiance values.*
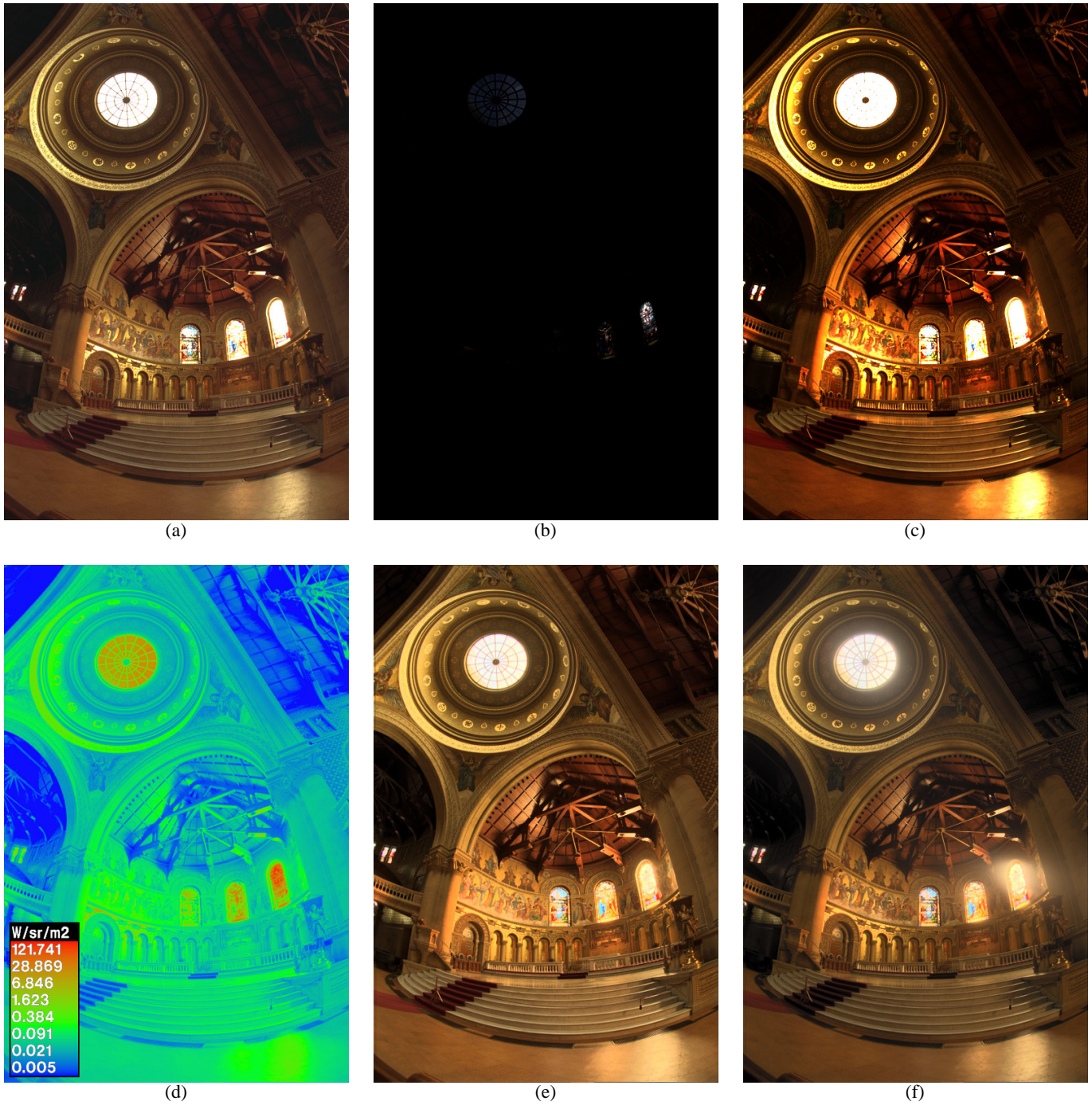
Figure 8: **(a)** *An actual photograph, taken with conventional print film at two seconds and scanned to PhotoCD.* **(b)** *The high dynamic range radiance map, displayed by linearly mapping its entire dynamic range into the dynamic range of the display device.* **(c)** *The radiance map, displayed by linearly mapping the lower* 0.1% *of its dynamic range to the display device.* **(d)** *A false-color image showing relative radiance values for a grayscale version of the radiance map, indicating that the map contains over five orders of magnitude of useful dynamic range.* **(e)** *A rendering of the radiance map using adaptive histogram compression.* **(f)** *A rendering of the radiance map using histogram compression and also simulating various properties of the human visual system, such as glare, contrast sensitivity, and scotopic retinal response. Images (e) and (f) were generated by a method described in [23]. Images (d-f) courtesy of Gregory Ward Larson.*

adjust the brightness and contrast of the images[10] to guarantee that each image would be digitized using the same response function.

An unfortunate aspect of the PhotoCD process is that it does not scan precisely the same area of each negative relative to the extents of the image.[11] To counteract this effect, we geometrically registered the images to each other using a using normalized correlation (see [4]) to determine, with sub-pixel accuracy, corresponding pixels between pairs of images.

Fig. 7(a-c) shows the response functions for the red, green, and blue channels of the church sequence recovered from 28 pixel locations. Fig. 7(d) shows the recovered red, green, and blue response curves plotted on the same set of axes. From this plot, we can see that while the red and green curves are very consistent, the blue curve rises significantly above the others for low exposure values. This indicates that dark regions in the images exhibit a slight blue cast. Since this artifact is modeled by the response curves, it will not affect the relative radiance values.

Fig. 8 interprets the recovered high dynamic range radiance map in a variety of ways. Fig. 8(a) is one of the actual photographs, which lacks detail in its darker regions at the same time that many values within the two rightmost stained glass windows are saturated. Figs. 8(b,c) show the radiance map, linearly scaled to the display device using two different scaling factors. Although one scaling factor is one thousand times the other, there is useful detail in both images. Fig. 8(d) is a false-color image showing radiance values for a grayscale version of the radiance map; the highest listed radiance value is nearly 250,000 times that of the lowest. Figs. 8(e,f) show two renderings of the radiance map using a new tone reproduction algorithm [23]. Although the rightmost stained glass window has radiance values over a thousand times higher than the darker areas in the rafters, these renderings exhibit detail in both areas.
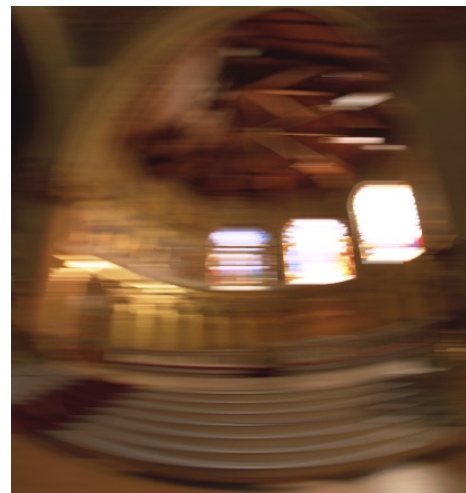
Figure 9 demonstrates two applications of the techniques presented in this paper: accurate signal processing and virtual photography. The task is to simulate the effects of motion blur caused by moving the camera during the exposure. Fig. 9(a) shows the results of convolving an actual, low-dynamic range photograph with a 37×1 pixel box filter to simulate horizontal motion blur. Fig. 9(b) shows the results of applying this same filter to the high dynamic range radiance map, and then sending this filtered radiance map back through the recovered film response functions using the same exposure time Δt as in the actual photograph. Because we are seeing this image through the actual image response curves, the two left images are tonally consistent with each other. However, there is a large difference between these two images near the bright spots. In the photograph, the bright radiance values have been clamped to the maximum pixel values by the response function. As a result, these clamped values blur with lower neighboring values and fail to saturate the image in the final result, giving a muddy appearance.

In Fig. 9(b), the extremely high pixel values were represented properly in the radiance map and thus remained at values above the level of the response function's saturation point within most of the blurred region. As a result, the resulting virtual photograph exhibits several crisply-defined saturated regions.
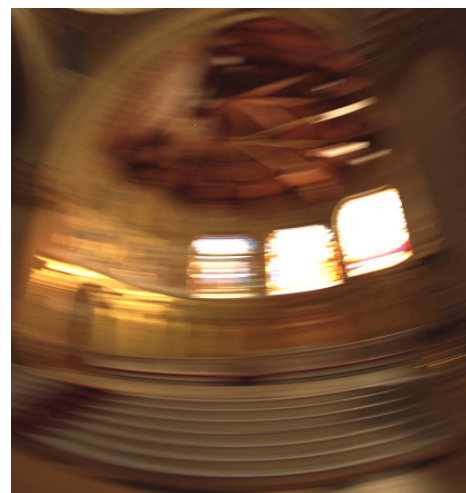
Fig. 9(c) is an actual photograph with real motion blur induced by spinning the camera on the tripod during the exposure, which is equal in duration to Fig. 9(a) and the exposure simulated in Fig. 9(b). Clearly, in the bright regions, the blurring effect is qualitatively similar to the synthetic blur in 9(b) but not 9(a). The precise shape of the real motion blur is curved and was not modeled for this demonstration.

---

[10]This feature of the PhotoCD process is called "Scene Balance Adjustment", or SBA.

[11]This is far less of a problem for cinematic applications, in which the film sprocket holes are used to expose and scan precisely the same area of each frame.

(a) Synthetically blurred digital image

(b) Synthetically blurred radiance map

(c) Actual blurred photograph

Figure 9: **(a)** *Synthetic motion blur applied to one of the original digitized photographs. The bright values in the windows are clamped before the processing, producing mostly unsaturated values in the blurred regions.* **(b)** *Synthetic motion blur applied to a recovered high-dynamic range radiance map, then virtually rephotographed through the recovered film response curves. The radiance values are clamped to the display device* after *the processing, allowing pixels to remain saturated in the window regions.* **(c)** *Real motion blur created by rotating the camera on the tripod during the exposure, which is much more consistent with (b) than (a).*

4 Conclusion

We have presented a simple, practical, robust and accurate method of recovering high dynamic range radiance maps from ordinary photographs. Our method uses the constraint of sensor reciprocity to derive the response function and relative radiance values directly from a set of images taken with different exposures. This work has a wide variety of applications in the areas of image-based modeling and rendering, image processing, and image compositing, a few of which we have demonstrated. It is our hope that this work will be able to help both researchers and practitioners of computer graphics make much more effective use of digitized photographs.

Acknowledgments

References

[1] ADAMS, A. *Basic Photo*, 1st ed. Morgan & Morgan, Hastings-on-Hudson, New York, 1970.

[2] CHEN, E. QuickTime VR - an image-based approach to virtual environment navigation. In *SIGGRAPH '95* (1995).

[3] DEBEVEC, P. E., TAYLOR, C. J., AND MALIK, J. Modeling and rendering architecture from photographs: A hybrid geometry- and image-based approach. In *SIGGRAPH '96* (August 1996), pp. 11–20.

[4] FAUGERAS, O. *Three-Dimensional Computer Vision*. MIT Press, 1993.

[5] FERWERDA, J. A., PATTANAIK, S. N., SHIRLEY, P., AND GREENBERG, D. P. A model of visual adaptation for realistic image synthesis. In *SIGGRAPH '96* (1996), pp. 249–258.

[6] GORTLER, S. J., GRZESZCZUK, R., SZELISKI, R., AND COHEN, M. F. The Lumigraph. In *SIGGRAPH '96* (1996), pp. 43–54.

[7] HORN, B. K. P. *Robot Vision*. MIT Press, Cambridge, Mass., 1986, ch. 10, pp. 206–208.

[8] JAMES, T., Ed. *The Theory of the Photographic Process*. Macmillan, New York, 1977.

[9] KAUFMAN, J. E., Ed. *IES Lighting Handbook; the standard lighting guide*, 7th ed. Illuminating Engineering Society, New York, 1987, p. 24.

[10] KOLB, C., MITCHELL, D., AND HANRAHAN, P. A realistic camera model for computer graphics. In *SIGGRAPH '95* (1995).

[11] LAVEAU, S., AND FAUGERAS, O. 3-D scene representation as a collection of images. In *Proceedings of 12th International Conference on Pattern Recognition* (1994), vol. 1, pp. 689–691.

[12] LEVOY, M., AND HANRAHAN, P. Light field rendering. In *SIGGRAPH '96* (1996), pp. 31–42.

[13] MADDEN, B. C. Extended intensity range imaging. Tech. rep., GRASP Laboratory, University of Pennsylvania, 1993.

[14] MANN, S., AND PICARD, R. W. Being 'undigital' with digital cameras: Extending dynamic range by combining differently exposed pictures. In *Proceedings of IS&T 46th annual conference* (May 1995), pp. 422–428.

[15] MCMILLAN, L., AND BISHOP, G. Plenoptic Modeling: An image-based rendering system. In *SIGGRAPH '95* (1995).

[16] SCHLICK, C. Quantization techniques for visualization of high dynamic range pictures. In *Fifth Eurographics Workshop on Rendering (Darmstadt, Germany)* (June 1994), pp. 7–18.

[17] SZELISKI, R. Image mosaicing for tele-reality applications. In *IEEE Computer Graphics and Applications* (1996).

[18] TANI, T. *Photographic sensitivity : theory and mechanisms*. Oxford University Press, New York, 1995.

[19] THEUWISSEN, A. J. P. *Solid-state imaging with charge-coupled devices*. Kluwer Academic Publishers, Dordrecht; Boston, 1995.

[20] TUMBLIN, J., AND RUSHMEIER, H. Tone reproduction for realistic images. *IEEE Computer Graphics and Applications 13*, 6 (1993), 42–48.

[21] WARD, G. J. Measuring and modeling anisotropic reflection. In *SIGGRAPH '92* (July 1992), pp. 265–272.

[22] WARD, G. J. The radiance lighting simulation and rendering system. In *SIGGRAPH '94* (July 1994), pp. 459–472.

[23] WARD, G. J., RUSHMEIER, H., AND PIATKO, C. A visibility matching tone reproduction operator for high dynamic range scenes. Tech. Rep. LBNL-39882, Lawrence Berkeley National Laboratory, March 1997.

A Matlab Code

Here is the MATLAB code used to solve the linear system that minimizes the objective function $\mathcal{O}$ in Equation 3. Given a set of observed pixel values in a set of images with known exposures, this routine reconstructs the imaging response curve and the radiance values for the given pixels. The weighting function $w(z)$ is found in Equation 4.

```
%
% gsolve.m - Solve for imaging system response function
%
% Given a set of pixel values observed for several pixels in several
% images with different exposure times, this function returns the
% imaging system's response function g as well as the log film irradiance
% values for the observed pixels.
%
% Assumes:
%
%   Zmin = 0
%   Zmax = 255
%
% Arguments:
%
%   Z(i,j) is the pixel values of pixel location number i in image j
%   B(j)   is the log delta t, or log shutter speed, for image j
%   l      is lamdba, the constant that determines the amount of smoothness
%   w(z)   is the weighting function value for pixel value z
%
% Returns:
%
%   g(z)   is the log exposure corresponding to pixel value z
%   lE(i)  is the log film irradiance at pixel location i

function [g,lE]=gsolve(Z,B,l,w)

n = 256;

A = zeros(size(Z,1)*size(Z,2)+n+1,n+size(Z,1));
b = zeros(size(A,1),1);

%% Include the data-fitting equations

k = 1;
for i=1:size(Z,1)
  for j=1:size(Z,2)
    wij = w(Z(i,j)+1);
    A(k,Z(i,j)+1) = wij;  A(k,n+i) = -wij;      b(k,1) = wij * B(i,j);
    k=k+1;
  end
end

%% Fix the curve by setting its middle value to 0

A(k,129) = 1;
k=k+1;

%% Include the smoothness equations

for i=1:n-2
  A(k,i)=l*w(i+1);        A(k,i+1)=-2*l*w(i+1);  A(k,i+2)=l*w(i+1);
  k=k+1;
end

%% Solve the system using SVD

x = A\b;

g = x(1:n);
lE = x(n+1:size(x,1));
```